frontiers | Frontiers in Chemistry

TYPE Original Research
PUBLISHED 24 November 2022
DOI 10.3389/fchem.2022.1093073

OPEN ACCESS

EDITED BY
He Xiaojun,
Wenzhou Medical University, China

REVIEWED BY
Jianxun Ding,
Changchun Institute of Applied Chemistry (CAS), China
Kelong Fan,
Institute of Biophysics (CAS), China

*CORRESPONDENCE
Zheng Lian,
20052430@ppsuc.edu.cn

SPECIALTY SECTION
This article was submitted to Medicinal and Pharmaceutical Chemistry, a section of the journal Frontiers in Chemistry

RECEIVED 08 November 2022
ACCEPTED 14 November 2022
PUBLISHED 24 November 2022

CITATION
Lian Z, Lu C, Zhu J, Zhang X, Wu T, Xiong Y, Sun Z and Yang R (2022), Mo@ZIF-8 nanozyme preparation and its antibacterial property evaluation. *Front. Chem.* 10:1093073. doi: 10.3389/fchem.2022.1093073

Mo@ZIF-8 nanozyme preparation and its antibacterial property evaluation

Zheng Lian[1,2]*, Chunqing Lu[1], Jiangqi Zhu[1,3], Xining Zhang[2], Ting Wu[2], Youlin Xiong[2], Zhiyi Sun[1] and Rong Yang[2]

[1]School of Criminal Investigation, People's Public Security University of China, Beijing, China, [2]CAS Key Laboratory for Biomedical Effects of Nanomaterials and Nanosafety, Center of Materials Science and Optoelectronics Engineering, CAS Center for Excellence in Nanoscience, National Center for Nanoscience and Technology, University of Chinese Academy of Sciences, Beijing, China, [3]Institute of Evidence Law and Forensic Science, China University of Politic Science and Law, Beijing, China

Types of nanozymes can produce free radicals and/or reactive oxygen species (ROS) to serve as broad spectrum antibacterial materials. Developing nanozyme-based antibacterial materials with good biocompatibility exhibits promising application prospects. In this study, we doped Mo to ZIF-8 (both components have good biocompatibility) to prepare a new nanozyme, Mo@ZIF-8, which can produce hydroxyl radicals (•OH) triggered by a low dosage of hydrogen peroxide (H_2O_2), exhibiting effective antibacterial capability against both Gram-negative bacteria (*Escherichia coli*) and Gram-positive bacteria (*Staphylococcus aureus*). This work provides a reference for the design of antibacterial nanozymes with good biocompatibility.

KEYWORDS

peroxidase-like nanozyme, metal organic framework, ZIF-8, molybdenum, antibacterial therapy

1 Introduction

Bacterial-related diseases has been one of public safety issues that greatly threaten the health of humankind. (Reverter et al., 2020; Yu et al., 2022; Ding et al., 2022). Antibiotics have been the most widely accepted treatment for bacterial infection diseases. (Stracy et al., 2022). However, the abuse of antibiotics attribute to the emergence of drug-resistant bacteria, which may threaten the global health and environment. (Lakemeyer et al., 2018; Serwecińska, 2020). Therefore, effective and broad-spectrum antibacterial agents are urgently needed.

Currently, types of materials, such as metals (Gu et al., 2020; Tian et al., 2021), metal oxides (Li et al., 2018; Dong et al., 2022), carbon materials (Bi et al., 2022), single-atom materials (Cai et al., 2022) and MXenes (Yu et al., 2022b), have been verified to have peroxidase (POD)-like activity when they are fabricated to nanoscale. These nanozymes can convert H_2O_2 into OH radicals to effectively kill bacteria.

Metal organic frameworks (MOFs) have large surface area and pore structures, which provides scaffold for the enzymatic (catalytic) performance. (Ma et al., 2020). Here, we developed a new type of antibacterial nanozyme (Mo@ZIF-8) by doping Mo to ZIF-8.

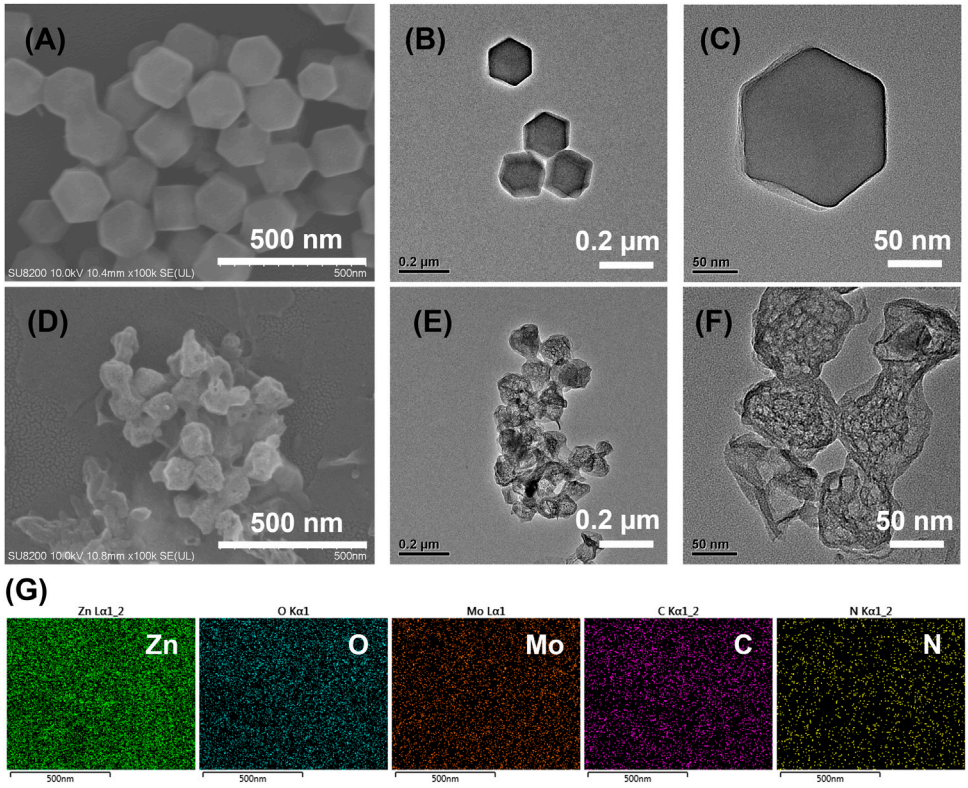

FIGURE 1
Characterizations of nanostructures from electron microscopy technique. **(A)** SEM image of ZIF-8. **(B,C)** TEM images of ZIF-8 at different magnifications. **(D)** SEM image of Mo@ZIF-8. **(E,F)** TEM images of Mo@ZIF-8 at different magnifications. **(G)** EDX analysis of Mo@ZIF-8. The images indicated that Mo had been doped to the nanostructures.

Briefly, the prepared hexahedron-shaped ZIF-8 (150 nm) was refluxed with Na_2MoO_4 solution and subsequent pyrolyzed at 600°C. The prepared Mo@ZIF-8 exhibited promising capability producing •OH and killing both Gram-negative (*E. coli*) and Gram-positive (*S. aureus*) bacteria at a low dosage of H_2O_2 (10^{-5} M). Due to the high biocompatibility of Mo and ZIF-8, this rationally designed nanozyme has the potential to be an effective antibacterial agent.

2 Experimental

2.1 Synthesis of hollow Mo@ZIF-8 nanostructures

0.595 g $Zn(NO_3)_2{\cdot}6H_2O$ was dissolved in 20 mL methanol (solution A). 0.656 g 2-methylimidazole (2-MIM) was dissolved in 20 mL methanol (solution B). Then solution B was rapidly added into solution A under vigorous for 15 min stirring at room temperature. The mixed solution was stand for 3 h at room temperature. After washing with methanol for three times, the white powder was collected by centrifugation and dried at 40°C.

To prepare Mo@ZIF-8 nanostructures, 0.075 g of as-prepared ZIF-8 was dispersed in 30 mL ethanol. Then 15 mL of Na_2MoO_4 solution (containing 0.0375 g $Na_2MoO_4{\cdot}2H_2O$) was mixed with ZIF-8 solution, then the mixed suspension refluxed at 82°C for 2 h. The precipitation was collected and wash by methanol for three times. The product was dried at 40°C and further annealed in Argon atmosphere at 600°C for 2 h with the rate of 5°C/min.

2.2 Enzyme-like activity and catalytic kinetics studies

The peroxidase-like activity of Mo@ZIF-8 nanostructures was tested by 3,3′,5,5′-tetramethylbenzidine (TMB) as substrate in the presence of H_2O_2. First, the Mo@ZIF-8 catalysts were dispersed in water with ultrasonication. Then, 1 mg/mL (50 μl) suspension was added to 450 μl NaAc–HAc buffer (0.1 M pH 3.0) containing 1 mM TMB and 2 mM H_2O_2. After incubation at room temperature for 20 min, the UV-vis absorption of the mixture was recorded. The influence of pH (2–9) and temperature (20–80°C) on the catalytic performance of Mo@ZIF-8 were also evaluated.

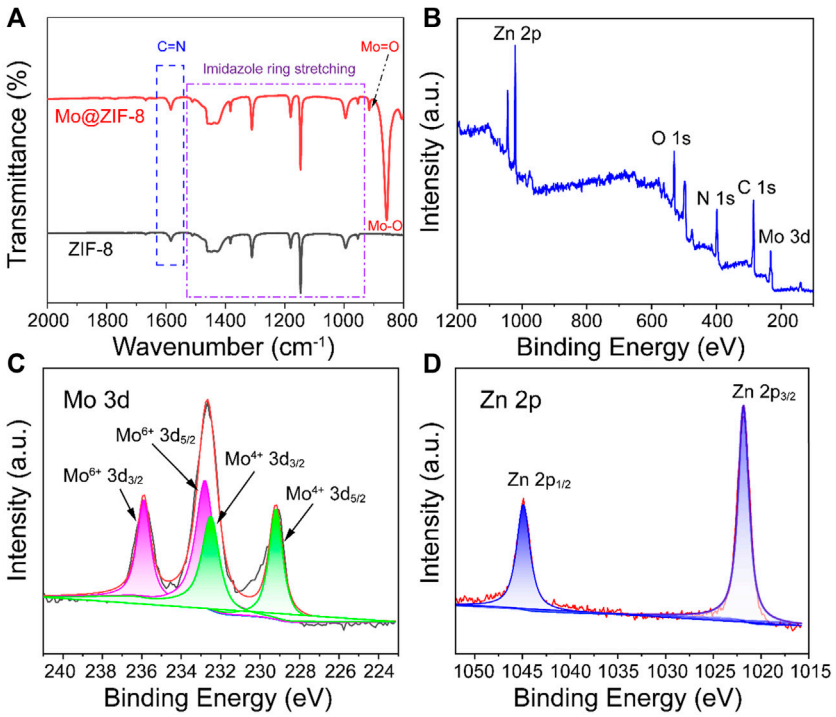

FIGURE 2
Characterizations of Mo@ZIF-8. **(A)** The FT-IR spectra of ZIF-8 and Mo@ZIF-8. The stretching peaks in the ZIF-8 and Mo@ZIF-8 were labeled. **(B–D)** XPS spectra of Mo@ZIF-8. **(B)** Survey spectrum. High-resolution XPS spectra of **(C)** Mo 3d, **(D)** Zn 2p.

The steady-stated kinetic experiments were carried out in 500 μL NaAc–HAc buffer (0.1 M pH 3.0) containing 100 μg/mL Mo@ZIF-8, 1 mM TMB and H_2O_2 ranging from 0 to 2.0 mM, or containing 100 μg/mL Mo@ZIF-8, 2 mM H_2O_2 and TMB ranging from 0 to 2.0 mM. The absorbance changes at 652 nm were constantly monitored in time-scan mode. The kinetic parameters were determined by the following equation:

$$\frac{1}{v} = \left(\frac{K_m}{V_{max}}\right)\left(\frac{1}{[S]}\right) + \frac{1}{V_{max}} \quad (1)$$

where v was the initial velocity, V_{max} was the maximal reaction velocity, K_m was the Michaelis–Menten constant and [S] was the substrate (TMB or H_2O_2) concentration, respectively.

2.3 Antibacterial experiments

Gram-positive *S. aureus* and Gram-negative *E. coli* were used for the antibacterial experiments. Typically, the experiments for each bacterium were divided into four groups: 1) bacteria, 2) bacteria + H_2O_2, 3) bacteria + Mo@ZIF-8, 4) bacteria + Mo@ZIF-8 + H_2O_2. The concentration of H_2O_2 used in the process was 10^{-5} M and the concentration of Mo@ZIF-8 was 2, 5 and 10 μg/mL. The bacteria were incubated with above solution for 4 h, then 30 μl of the suspension (1.0×10^7 CFU/mL *S. aureus* or *E. coli*) were spread on Luria-Bertani (LB) solid medium. These plates were kept at 37°C for 18 h, and bacterial colonies were counted.

Scanning electron microscopy (SEM) was used to observe the morphological change of the bacteria after antibacterial experiments. Groups: 1) control (bacteria without any treatment), 2) 10^{-5} M H_2O_2, 3) 5 μg/mL Mo@ZIF-8, 4) 5 μg/mL Mo@ZIF-8 + 10^{-5} M H_2O_2. After incubated for 4 h, the bacterial suspensions were collected and dropped onto silicon slides. Subsequently, bacterial cells were prefixed with 2.5% glutaraldehyde for 4 h, and dehydrated by a graded series of ethanol (30%, 50%, 70%, 80%, 90%, and 100%, respectively). The bacteria were finally dried for observation by scanning electron microscope.

3 Results and discussion

3.1 Structure characterizations

The SEM and TEM characterizations showed a hexahedron shape for ZIF-8 with the size of about 150 nm. (Figures 1A–C).

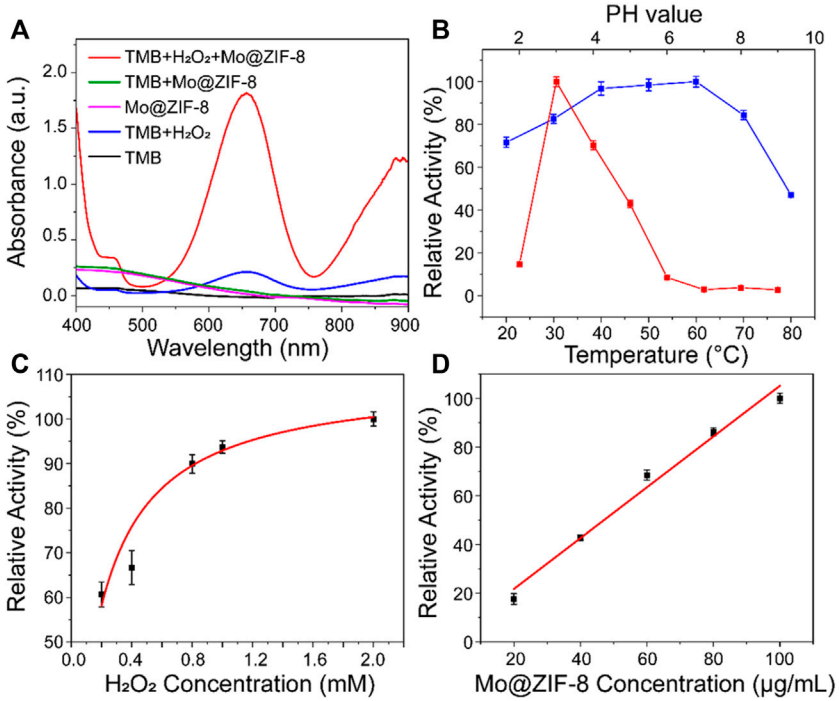

FIGURE 3
The peroxidase-like activity of the Mo@ZIF-8. **(A)** Absorbance spectra of TMB in different systems. **(B)** pH (red) and temperature (blue) dependence of Mo@ZIF-8 peroxidase activity. **(C)** H_2O_2 concentration dependence of the peroxidase-like activity of Mo@ZIF-8. **(D)** Concentration dependence of peroxidase activity of Mo@ZIF-8. In **(B–D)**, data are presented as mean ± SD (n = 3).

Meanwhile, TEM images showed the smooth surface of the ZIF-8 crystals (Figures 1B,C). After refluxing with Na_2MoO_4, the product became rounded and the corner disappeared. The size of the product was smaller than ZIF-8, which was about 100 nm. (Supplementary Figure S1A,B). The product was annealed at 600°C in Argon atmosphere and Mo@ZIF-8 formed. The Mo@ZIF-8 exhibited rough surfaces and hollow structures, shown in Figures 1D–F. TEM revealed their hollow and spongy structure, and the average diameter of the Mo@ZIF-8 was about 100 nm. (Figure 1F).

The incorporation of Mo element into ZIF-8 was confirmed by Energy Dispersive X-Ray Spectroscopy (EDX). The element distribution of Mo@ZIF-8 was shown in Figure 1G, demonstrating a homogeneous distribution of Zn, O, Mo, C, N elements in the nanocomposites.

FT-IR spectra of ZIF-8 and Mo@ZIF-8 were performed to demonstrate the successful incorporation of Mo, as shown in Figure 2A. The FT-IR spectra of ZIF-8 and Mo@ZIF-8 exhibited the characteristic peaks of 953–1,511 cm^{-1} and 1,582 cm^{-1}, which corresponded to the signals of the imidazole ring stretching and C=N bond of ZIF-8. (Wang et al., 2016; Zhang and Park, 2019). This revealed that the introduction of Mo did not destroy the imidazole ring. For the Mo@ZIF-8, new peaks appeared at 857 cm^{-1} and 916 cm^{-1}, which might be attributed to the stretching vibration of Mo-O and Mo=O bond, respectively. (Lin et al., 2020).

Furthermore, X-ray photoelectron spectroscopy (XPS) was explored the chemical composition and element valence state of Mo@ZIF-8 nanocomposites. Wide-scan XPS spectrum (Figure 2B) indicated the presence of C, O, N, Zn, and Mo in the Mo@ZIF-8 nanocomposites, confirming that Mo was successfully loaded on ZIF-8. Figure 2C was the high-resolution XPS spectrum of Mo 3d. Three bands at 235.9 , 232.6, and 229.2 eV could be assigned to Mo 3d doublets. The fitted Mo 3d peaks positioned at 229.2 and 232.5 eV were corresponding to Mo (IV). While, the doublet peaks at 232.8 and 235.9 eV were indexed to Mo (VI). (Zheng et al., 2017; Lian et al., 2022). As displayed in Figure 2D, the binding energy for Zn 2p3/2 and 2p1/2 were 1,021.8 and 1,044.8 eV, respectively. (Hua et al., 2019).

3.2 The peroxidase mimetic activity of Mo@ZIF-8

TMB, a classical chromogenic substrate, was used to test the peroxide-like activity of Mo@ZIF-8 nanocomposites in the presence of H_2O_2. (Wang et al., 2019). As shown in Figure 3A, Mo@ZIF-8 exhibited highest absorbance at 652 nm, illustrating the high peroxidase-like activity. However, ZIF-8 showed negligible enzymatic activity under the same

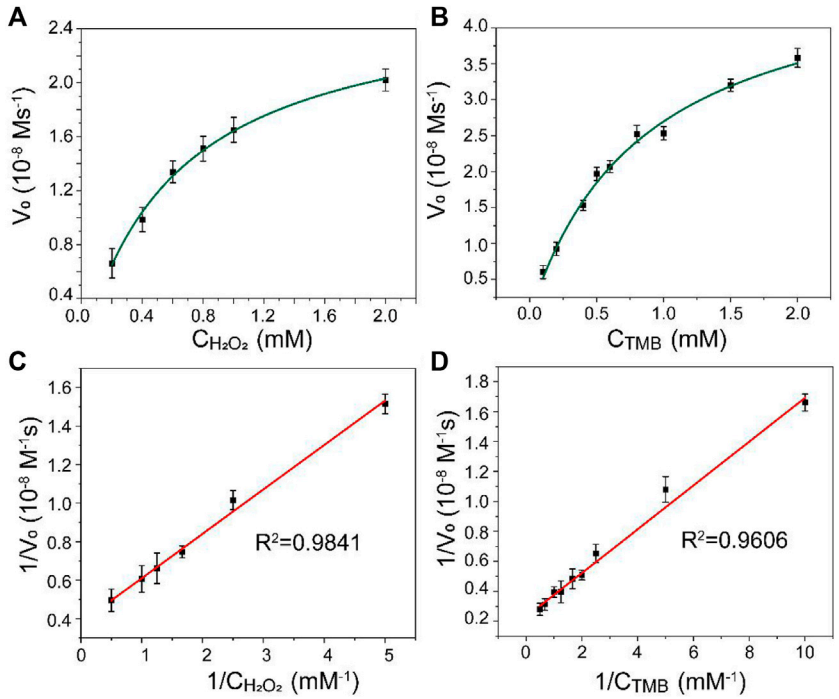

FIGURE 4
Steady-state kinetic analysis for Mo@ZIF-8-catalyzed TMB oxidation. **(A,B)** Michaelis–Menten model analysis. **(C,D)** Lineweaver–Burk models analysis. Data are presented as mean ± SD (n = 3).

condition, (Supplementary Figure S2), which indicated that the introduction of Mo element played a key role during the catalytic process. In contrast, H_2O_2 alone did not show significant absorption at 652 nm. The catalytic performance of enzyme was highly dependent on pH, temperature, concentration of H_2O_2 and nanozyme. Experiments were carried out at different pH (2–9) and temperature (20–80°C), and the optimum condition for the peroxide-like activity of Mo@ZIF-8 was found to be pH 3 and 60°C. (Figure 3B). Notably, Mo@ZIF-8 exhibited high catalytic activity in a broad temperature range, illustrating its low sensitivity towards temperature. Furthermore, the catalytic activity of Mo@ZIF-8 was directly enhanced by the increasing concentration of H_2O_2 (Figure 3C). And there was almost a linear relationship between the concentration of Mo@ZIF-8 and its relative catalytic activity (Figure 3D).

The kinetic analysis of Mo@ZIF-8 was further investigated using steady-state kinetic experiments. The data were collected by using a series of TMB concentrations with constant H_2O_2 concentration and *vice versa*. The Michaelis–Menten constant (K_m) and the maximum initial velocity (V_{max}) could be calculated from Lineweaver–Burk double reciprocal plots, which showed a good linear-ship between v^{-1} and $[S]^{-1}$. (Figure 4). The K_m values of Mo@ZIF-8 were 0.62 and 0.86 mM with H_2O_2 and TMB as the substrates, respectively, and the corresponding V_{max} values were 26.64 nM s^{-1} and 50.15 nM s^{-1}.

The mechanism of Mo@ZIF-8 peroxidase-like activity was investigated. Assuming that Mo@ZIF-8 could convert H_2O_2 into hydroxyl radicals (•OH) through the POD-like activity, terephthalic acid (TA) was used to confirm the production of •OH during the catalytic progress. TA was a nonfluorescent molecule, but it could easily react with •OH to generate highly fluorescent 2-hydroxy terephthalic acid. (Wang et al., 2018). As shown in Supplementary Figure S3, the enhancement in fluorescence intensity was significant when compared with the control group, confirming the production of hydroxyl radicals by Mo@ZIF-8 in the presence of H_2O_2. All the results indicated that Mo@ZIF-8 showed POD enzyme mimicking activity and was suitable and efficient for killing bacteria.

3.3 Antibacterial experiments

The antibacterial effect of the Mo@ZIF-8 nanocomposites was evaluated with the assistance of H_2O_2. The bacterial viability was measured by counting the colonies forming units. During the antibacterial experiments, the concentration of H_2O_2 was 10^{-5} M, which hardly affect the survival of both *E. coli* and *S. aureus*. Figure 5 showed the images of bacteria colonies on LB agar with various treatments. As shown, Mo@ZIF-8 alone showed a dose-dependent inhibition effect. However, Mo@ZIF-8 combined with low

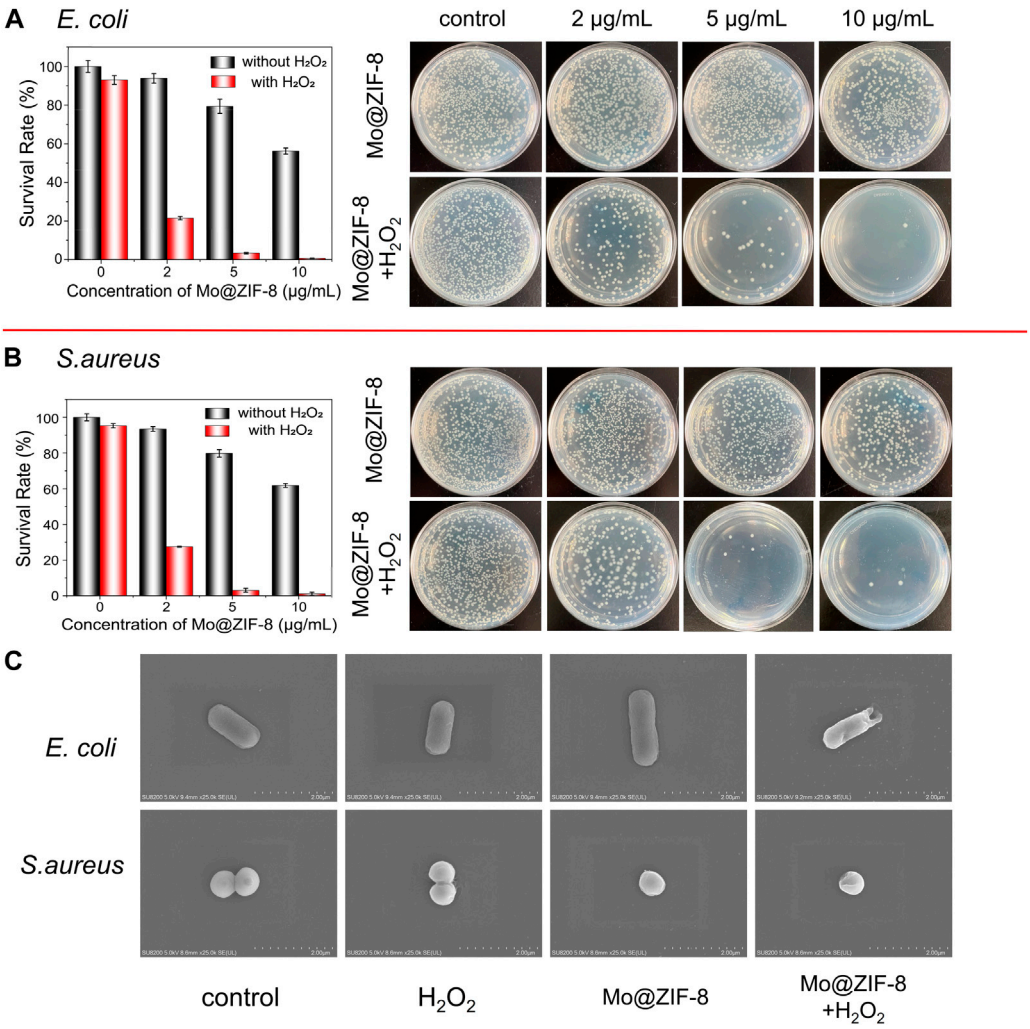

FIGURE 5
Antibacterial capability of Mo@ZIF-8. Bacterial proliferation and the corresponding images of bacterial colonies on LB agar at different concentration with and without H_2O_2. **(A)** Antibacterial capability of Mo@ZIF-8 to *E. coli* (Gram-negative). **(B)** Antibacterial capability of Mo@ZIF-8 to *S. aureus* (Gram-positive). In **(A)** and **(B)**, data are presented as mean ± SD (n = 3). **(C)** Representative morphologies of bacteria in different groups imaged by SEM.

concentration H_2O_2 (10^{-5} M) exhibited excellent antibacterial effect, and the inhibition efficiency towards *E. coli* and *S. aureus* reached to 99.2% and 99.4%, respectively, when the concentration of Mo@ZIF-8 was 10 μg/mL. These results illustrated that Mo@ZIF-8 could be used as an efficient antibacterial agent.

The morphological changes of *E. coli* and *S. aureus* were investigated after various treatment by SEM. In Figure 5C, as for *E. coli*, no obvious morphological change was observed in the control, H_2O_2 and Mo@ZIF-8 groups, and *E. coli* cells showed rod-shape, with intact and smooth cell walls. As for the groups with treatment of both Mo@ZIF-8 and H_2O_2, *E. coli* cells lost their cellular integrity, with noticeable holes on its cell wall. For *S. aureus*, the results were similar. *S. aureus* in the control, H_2O_2 and Mo@ZIF-8 groups exhibited a sphere shape, a well-defined and even cell wall. Nevertheless, the morphology of *S. aureus* cells incubated with Mo@ZIF-8 and H_2O_2 were changed. In this group, *S. aureus* cells were damaged, even with intracellular components leaked. These results demonstrated excellent antibacterial capability of Mo@ZIF-8 with the assistant of H_2O_2.

4 Conclusion

In summary, we fabricated a new nanozyme, Mo@ZIF-8 nanocomposites through refluxing Na_2MoO_4 solution with ZIF-8 and pyrolyzing at 600°C. This nanocomposite exhibited peroxide-like activity and achieved a wide range of antibacterial capability against both Gram-negative (*E. coli*) and Gram-

positive (*S. aureus*) bacteria through producing •OH. Due to the high biocompatibility of the selected components, Mo and ZIF-8, the Mo@ZIF-8 nanozyme has the potential to be an effective antibacterial agent applied in biomedical field.

Data availability statement

The original contributions presented in the study are included in the article/Supplementary Material, further inquiries can be directed to the corresponding author.

Author contributions

ZL: Methodology, formal analysis, investigation, writing—original draft, writing—review and editing, funding. CL: Formal analysis, methodology. JZ: investigation, resources. XZ: Formal analysis, investigation. TW: Formal analysis, investigation. YX: Formal analysis, investigation. ZS: Formal analysis. RY: Conceptualization, writing—review and editing, supervision, project administration.

Funding

This project was financially supported by the Fundamental Research Funds for the Central Universities (2021JKF210) awarded by the People's Public Security University of China.

Acknowledgments

The authors would like to express sincere thanks to the professors and technicists of National Center for Nanoscience and Technology for their supports and assistance.

Conflict of interest

The authors declare that the research was conducted in the absence of any commercial or financial relationships that could be construed as a potential conflict of interest.

Publisher's note

Supplementary material

The Supplementary Material for this article can be found online at: https://www.frontiersin.org/articles/10.3389/fchem.2022.1093073/full#supplementary-material

References

Bi, X., Bai, Q., Wang, L., Du, F., Liu, M., Yu, W. W., et al. (2022). Boron doped graphdiyne: A metal-free peroxidase mimetic nanozyme for antibacterial application. *Nano Res.* 15, 1446–1454. doi:10.1007/s12274-021-3685-4

Cai, S., Liu, J., Ding, J., Fu, Z., Li, H., Xiong, Y., et al. (2022). Tumor-microenvironment-Responsive cascade reactions by a cobalt-single-atom nanozyme for synergistic nanocatalytic chemotherapy. *Angew. Chem. Int. Ed. Engl.* 16, e202204502. doi:10.1002/anie.202204502

Ding, J., Xiao, H., and Chen, X. (2022). Advanced biosafety materials for prevention and theranostics of biosafety issues. *Biosaf. Health* 4, 59–60. doi:10.1016/j.bsheal.2022.03.011

Dong, H., Du, W., Dong, J., Che, R., Kong, F., Cheng, W., et al. (2022). Depletable peroxidase-like activity of Fe_3O_4 nanozymes accompanied with separate migration of electrons and iron ions. *Nat. Commun.* 13, 5365. doi:10.1038/s41467-022-33098-y

Gu, H., Huang, Q., Zhang, J., Li, W., and Fu, Y. (2020). Heparin as a bifunctional biotemplate for Pt nanocluster with exclusively peroxidase mimicking activity at near-neutral PH. *Colloids Surfaces A Physicochem. Eng. Aspects* 606, 125455. doi:10.1016/j.colsurfa.2020.125455

Hua, Y., Li, X., Zhang, X., Zhang, L., Shu, Y., Sheng, H., et al. (2019). Active anchoring polysulfides of ZnS-decorated porous carbon aerogel for a high-performance lithium-sulfur battery. *ChemElectroChem* 6, 2570–2577. doi:10.1002/celc.201900556

Lakemeyer, M., Zhao, W. N., Mandl, F. A., Hammann, P., and Sieber, S., and(2018). Thinking outside the box-novel antibacterials to tackle the resistance crisis. *Angew. Chem. Int. Ed.* 57, 14440–14475. doi:10.1002/anie.201804971

Li, D., Liu, B., Huang, P., Zhang, Z., and Liu, J. (2018). Highly active fluorogenic oxidase mimicking NiO nanozymes. *Chem. Commun.* 54, 12519–12522. doi:10.1039/c8cc07062h

Lian, Z., Li, H., Wu, T., Zhao, J., Cai, S., and Yang, R. (2022). Vapor deposition of MoO_x/MoS_2 films on silicon wafer with visible-light responsive photocatalytic antibacterial properties. *Appl. Surf. Sci.* 606, 154874. doi:10.1016/j.apsusc.2022.154874

Lin, Z., Zhang, X., Liu, S., Zheng, L., Bu, Y., Deng, H., et al. (2020). Colorimetric acid phosphatase sensor based on MoO_3 nanozyme. *Anal. Chim. Acta* 1105, 162–168. doi:10.1016/j.aca.2020.01.035

Ma, L., iang, F., Fan, X., Wang, L., He, C., Zhou, M., et al. (2020). Metal-organic-framework-engineered enzyme-mimetic catalysts. *Adv. Mat.* 32, e2003065. doi:10.1002/adma.202003065

Reverter, M., Sarter, S., Caruso, D., Avarre, J. C., Combe, M., Pepey, E., et al. (2020). Aquaculture at the crossroads of global warming and antimicrobial resistance. *Nat. Commun.* 11, 1870. doi:10.1038/s41467-020-15735-6

Serwecińska, L. (2020). Antimicrobials and antibiotic-resistant bacteria: A risk to the environment and to public health. *Water* 12, 3313. doi:10.3390/w12123313

Stracy, M., Snitser, O., Yelin, I., Amer, Y., Parizade, M., Katz, R., et al. (2022). Minimizing treatment-induced emergence of antibiotic resistance in bacterial infections. *Science* 375, 889–894. doi:10.1126/science.abg9868

Tian, Y., Chen, Y., Chen, M., Song, Z., Xiong, B., and Zhang, X. (2021). Peroxidase-like Au@Pt nanozyme as an integrated nanosensor for Ag^+ detection by LSPR spectroscopy. *Talanta* 221, 121627. doi:10.1016/j.talanta.2020.121627

Wang, H., Li, P., Yu, D., Zhang, Y., Wang, Z., Liu, C., et al. (2018). Unraveling the enzymatic activity of oxygenated carbon nanotubes and their application in the treatment of bacterial infections. *Nano Lett.* 18, 3344–3351. doi:10.1021/acs.nanolett.7b05095

Wang, H., Wan, K., and Shi, X. (2019). Recent advances in nanozyme research. *Adv. Mat.* 31, e1805368. doi:10.1002/adma.201805368

Wang, X., Liu, J., Leong, S., Lin, X., Wei, J., Kong, B., et al. (2016). Rapid construction of ZnO@ZIF-8 heterostructures with size-selective photocatalysis properties. *ACS Appl. Mat. Interfaces* 8, 9080–9087. doi:10.1021/acsami.6b00028

Yu, L., Chang, J., Zhuang, X., Li, H., Hou, T., and Li, F. (2022). Two-dimensional cobalt-doped Ti_3C_2 MXene nanozyme-mediated homogeneous electrochemical strategy for pesticides assay based on *in situ* generation of electroactive substances. *Anal. Chem.* 94, 3669–3676. doi:10.1021/acs.analchem.1c05300

Yu, Y., Ding, J., Zhou, Y., Xiao, H., and Wu, G. (2022). Biosafety chemistry and biosafety materials: A new perspective to solve biosafety problems. *Biosaf. Health* 4, 15–22. doi:10.1016/j.bsheal.2022.01.001

Zhang, Y., and Park, S. (2019). Facile construction of MoO_3@ZIF-8 core-shell nanorods for efficient photoreduction of aqueous Cr (VI). *Appl. Catal. B Environ.* 240, 92–101. doi:10.1016/j.apcatb.2018.08.077

Zheng, Z., Cong, S., Gong, W., Xuan, J., Li, G., Lu, W., et al. (2017). Semiconductor SERS enhancement enabled by oxygen incorporation. *Nat. Commun.* 8 (1), 1993. doi:10.1038/s41467-017-02166-z